This article has been accepted for inclusion in a future issue of this journal. Content is final as presented, with the exception of pagination.

Design, Manufacturing, and Experimental Characterization of a First-of-a-Kind DTT ECH Mirror Equipped With TPMS

Eleonora Gajetti, Alessandro Bruschi, Francesco Fanale, William Ferretto, Gustavo Granucci, Andrea Lucchini, Luca Marocco, Afra Romano, and Laura Savoldi, *Senior Member, IEEE*

***Abstract*—The design, manufacturing, and experimental characterization of the prototype of an electron cyclotron heating (ECH) mirror equipped with an innovative cooling system based on triply periodic minimal surfaces (TPMS) is presented here. The prototype, manufactured in AISI 316L via selective laser melting (SLM), is engineered to withstand high heat fluxes and to mitigate eddy currents induced during tokamak operation. The TPMS cooling structure features a Gyroid topology with variable cell size. Hydraulic and thermal tests were conducted in a dedicated water loop, and experimental results were compared to numerical predictions. The measured pressure drops were worse than those calculated, probably due to surface roughness and geometrical deviations, and can be reproduced numerically with a geometry with an effective porosity lower than the nominal one. The thermal measurements, on the other hand, appear to be quite far from the simulations, probably due to the influence of the experimental setup on the thermocouple readings. These findings confirm the potential of TPMS-based cooling for ECH mirrors and highlight areas for further improvement in manufacturing, modeling, and testing.**

***Index Terms*—Additive manufacturing, cooling, fusion reactor design, microwave generation, mirrors, triply periodic minimal surfaces (TPMS).**

I. Introduction

THE electron cyclotron heating (ECH) [1] system in fusion devices is engineered to transmit and direct high-power microwave beams—generated by megawatt-class gyrotrons [2]—into the plasma chamber using multiple mirrors [3]. In the Divertor Tokamak Test (DTT) [4] facility, under realization at the ENEA premises in Frascati, Rome, the ECH system will employ 32 gyrotrons [5] operating at 170 GHz, similar to those used in ITER [6], [7], [8], [9]. These gyrotrons are grouped into four clusters of eight units, with their output delivered through long, quasi-optical vacuum transmission lines to a total of eight front-steering antennas [10]. The microwave beams are launched into the plasma through two mirrors, M1 and M2.

Those mirrors are subject to significant heat loads with peaks of several MW/m^2 due to Joule dissipation from the reflected radiation. Additionally, the launcher mirrors, located in regions where the magnetic field is nonnegligible, are expected to experience eddy currents induced by the fast variation of the magnetic field during tokamak operation, in particular during plasma disruption [11]. As a consequence, they are subject to high torques, the extent of which depends on the electrical resistivity of the mirror material (the lower the resistivity, the higher the torque). In the case of steerable mirrors, the induced torque should be minimized. As an alternative option to highly electrically conductive Cu-alloys, a natural choice for highly effective cooling is thus envisaged for those mirrors, and AISI 316L was considered as a possible candidate material for the M2 mirror [12]. However, alternative materials, such as the mentioned AISI 316L, are characterized by worse thermal properties, thus requiring the most efficient cooling solutions to prevent deformations and stresses that could jeopardize the functionality of the device.

An emerging cooling technology exploiting the potential of additive manufacturing, implementing triply periodic minimal surfaces (TPMS), has recently been proposed to improve heat transfer [13] and enhance the overall performance of ECH mirrors [14]. TPMS are structured, periodic lattices characterized by a high surface-to-volume ratio [15] that is particularly advantageous for the removal of high heat fluxes, resulting in very promising cooling structures for the high heat flux components used in fusion machines [16].

A preliminary parametric numerical study on the thermal performance of TPMS-based cooling systems was conducted on a DTT ECH mirror in [14], where two TPMS topologies with different sizes and porosities were analyzed. In that study, several cooling system configurations were designed and numerically simulated to identify the optimal TPMS structure for ECH mirror cooling, although no experimental testing was

Received 30 September 2025; revised 20 February 2026; accepted 24 April 2026. This work was supported by the DTT Consortium. The review of this article was arranged by Senior Editor M. Kovari. *(Corresponding author: Eleonora Gajetti.)*

Eleonora Gajetti and Laura Savoldi are with the MAHTEP Group, Dipartimento Energia “Galileo Ferraris,” Politecnico di Torino, 10129 Turin, Italy (e-mail: eleonora.gajetti@polito.it).

Alessandro Bruschi and Francesco Fanale are with the Institute for Plasma Science and Technology, National Research Council (ISTP-CNR), 20125 Milan, Italy.

William Ferretto, Andrea Lucchini, and Luca Marocco are with the Dipartimento di Energia, Politecnico di Milano, 20156 Milan, Italy.

Gustavo Granucci is with the Institute for Plasma Science and Technology, National Research Council (ISTP-CNR), 20125 Milan, Italy, and also with DTT S.C.a r.l., 00044 Frascati (RM), Italy.

Afra Romano is with DTT S.C.a r.l., 00044 Frascati (RM), Italy, and also with the Fusion and Nuclear Safety Department, ENEA, 00044 Frascati, Italy.

Color versions of one or more figures in this article are available at https://doi.org/10.1109/TPS.2026.3700964.

Digital Object Identifier 10.1109/TPS.2026.3700964

© 2026 The Authors. This work is licensed under a Creative Commons Attribution 4.0 License.
For more information, see https://creativecommons.org/licenses/by/4.0/

This article has been accepted for inclusion in a future issue of this journal. Content is final as presented, with the exception of pagination.

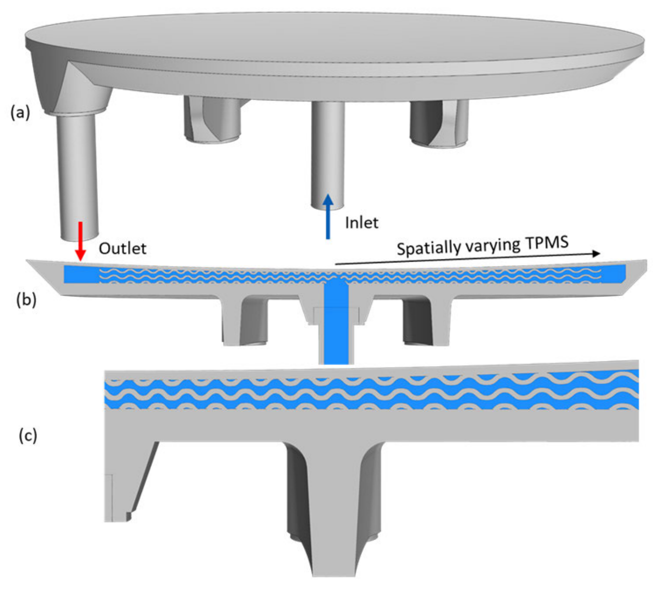

Fig. 1. Prototype mirror geometry. (a) Solid domain with inlet/outlet. (b) Cut section highlighting the varying TPMS. (c) Zoomed-in view of the cut section.

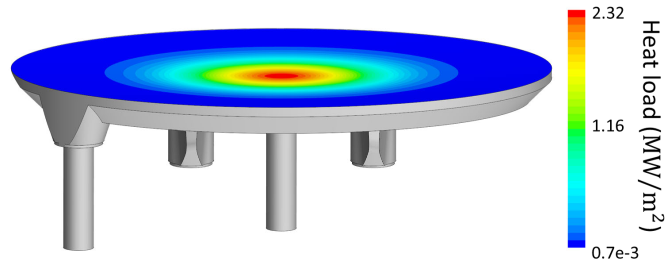

Fig. 2. Heat load on the reflective surface.

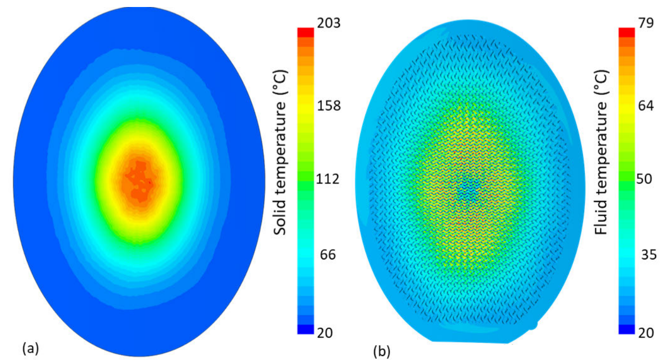

Fig. 3. Temperature map of (a) solid domain and (b) fluid domains, simulated in the nominal operating conditions at Falcon.

performed. Building on those numerical findings, the present work extends the investigation to the design, fabrication, and both numerical and experimental analysis of a prototype for the M2 mirror. For the first time, a TPMS-equipped AISI 316L mirror has been not only designed but also manufactured and experimentally tested. This completes the full workflow (from design to experimental testing), demonstrating the feasibility of using such structures.

II. Design and Simulation

A. Mirror Design

The designed prototype mirror is elliptical with a major radius of 89 mm and a minor radius of 63 mm. The design has targeted the compatibility with a connection line to be installed at the FALCON test facility at the EPFL premises in Lausanne, CH [17] for the tests of mirrors and other microwave components at high power. Such lines require a concave reflecting surface, so that, despite the fact that the DTT M2 mirror will have a flat surface, the designed prototype experiences a curved reflective 1-mm-wide layer. The cooling system consists of a Gyroid lattice in the central part of the mirror, where the Gaussian-shaped heat load is greatest. To guarantee a better homogeneity of the water flow to the single outlet and ensure more efficient depowdering during the manufacturing, an annular manifold surrounds the lattice at the outboard of the elliptical shape. The Gyroid lattice is designed with an increasing unit cell size moving outboard.

The set-level equation for the lattice is reported in (1), where $X = 2\pi x/\Lambda(x, y)$, $Y = 2\pi y/\Lambda(x, y)$, and $Z = 2\pi z/\Lambda(x, y)$. $\Lambda(x, y)$ is a function varying with the mirror surface concavity. To design the actual lattice, the characteristic in (1) is offset toward the two normal directions of a varying coefficient $c(x, y)$, as in (2). The cell size changes from 3 mm in the center to about 4.5 mm in the most peripheral parts. The minimum wall thickness, in the center, is around 0.8 mm, for a $c = 0.75$. The resulting porosity is $\varphi = 48\%$

$$f(x, y, z) = sin(X)\,cos(Y) + sin(Y)\,cos(Z) + sin(Z)\,cos(X) \tag{1}$$

$$(f(x, y, z) - c(x, y)) \cup (f(x, y, z) + c(x, y)). \tag{2}$$

The geometry of the prototype mirror is shown in Fig. 1(a), and a detail of the increasing TPMS cell size can be appreciated in Fig. 1(b) and (c).

B. Design Performance

The thermal-hydraulic performance of prototype mirror has been initially evaluated in the operating conditions of the Falcon facility (inlet water flow rate of 10 L/min at 20 °C and Gaussian heat flux with peak of 2.3 MW/m^2, see Fig. 2) to verify the compliance to requirements, i.e., maximum fluid temperatures below saturation point at 3–7 bar (minimum and maximum operating pressure levels) and pressure drop lower than 4 bar. The thermal–hydraulic steady-state simulations have been performed using STAR-CCM+ [18], using the $k - \varepsilon$ Realizable turbulence model. A polyhedral mesh has been used, with boundary layers to capture the near-wall behavior. Due to the tiny features of the TPMS, a very fine grid has been generated, with 84 M cells. The conjugate heat transfer problem is solved with temperature-dependent properties for both subcooled water and mirror steel. The heat flux shown in Fig. 2 is used as the thermal driver, with all the other mirror boundaries adiabatic.

Fig. 3 shows the temperature fields on the reflective layer and at the fluid–solid interface underneath the reflective layer.

This article has been accepted for inclusion in a future issue of this journal. Content is final as presented, with the exception of pagination.

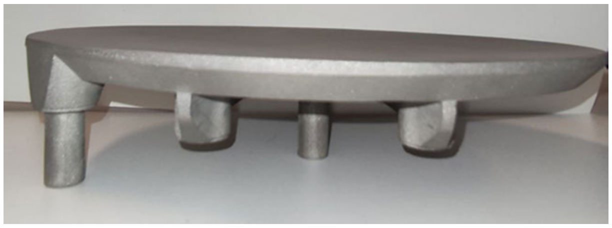

Fig. 4. 3-D printed mirror after manufacturing and depowdering.

The maximum solid temperature remains well below the softening point of the AISI 316L of 700 ° C [19]. The maximum fluid temperature does not exceed the saturation temperature at 3 bar, the minimum pressure level, estimated in 133 ° C [20].

The reflective layer temperature follows the Gaussian shape of the heat flux, while the fluid–solid interface temperature shows the influence of cooling effects. In particular, the impinging of the fluid arriving with a velocity of 3.3 m/s from the inlet connection is clearly visible. The temperature fields do not present significant inhomogeneity due to the presence of the single outlet, although in Fig. 3(b) the location of the outlet at the bottom right corner in the shown map is revealed by the decrease of fluid temperature. The computed pressure drop at the nominal flow rate is 2.7 bar.

III. Manufacturing

The prototype mirror was printed via additive manufacturing using the laser powder bed fusion (LPBF) method—also called selective laser melting (SLM)—by the private company Ellena S.p.A., employing a 240-W printer with a spot of 0.1 mm. The resulting part accuracy and surface roughness estimated by the manufacturer are 0.15 mm and 5 – 15 μm, respectively. The company also evaluated the relative part density around 99.85% of the bulk material, which ensures that mechanical properties have not been degraded because of porosity decrease in metal [21].

The sample was successfully depowdered using a vibrating machine, manually shaken with a rubber hammer, and by injecting compressed air and pressurized water, as well as employing an industrial ultrasonic washing machine. The outer surface of the sample is shown in Fig. 4.

IV. Testing

In order to test the mirror design, a preliminary experimental campaign was conducted at the thermal-hydraulic laboratory *Frigorifero* at Politecnico di Milano, Milan, Italy. Both hydraulic and thermal tests were carried out in a dedicated water loop in order to compare the numerical results with the experimental ones and check the predictability of the model.

A. Experimental Setup

A picture of the experimental hydraulic circuit is shown in Fig. 5, while its operating scheme, including the thermal components, is reported in Fig. 6. With reference to Fig. 6, the water loop is composed of a centrifugal pump (*P*); a flow control valve (*V*); a Coriolis mass flowmeter (*MF*); a heat

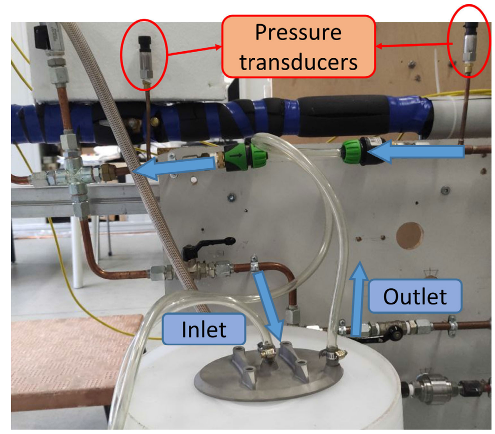

Fig. 5. Hydraulic circuit at the *Frigorifero* Laboratory, Department of Energy, Politecnico di Milano, used for the experimental testing of the mirror prototype.

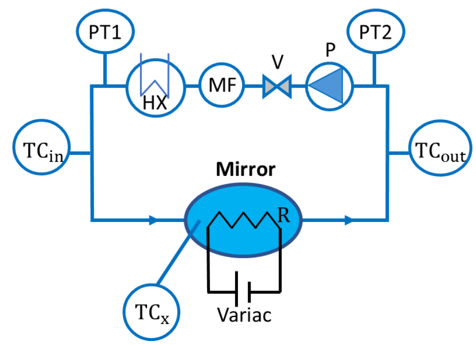

Fig. 6. Sketch of the equivalent circuit of the experimental setup.

TABLE I
Measuring Instruments

Type	Range	Accuracy
Mass flow meter 1	0 - 6.7 l/min	0.15% r.v.
Mass flow meter 2	0 - 108 l/min	0.3% r.v.
Relative pressure transducer	0.5 - 7 bar	0.07 bar
Type K thermocouples	0-50°C	0.5 °C

exchanger (*HX*) that is fed by a secondary cooling loop to maintain a constant water outlet temperature; and two relative pressure transducers (*PT1* and *PT2*) and two thermocouples (TC_{in} and TC_{out}) are employed to measure the pressure and temperature upstream and downstream the test section of the mirror. The mirror is connected to the loop via 10-mm-diameter transparent plastic tubes to the circuit. A resistor (*R*) connected to a variac (an autotransformer employed to impose the voltage difference applied to the resistor terminals) is used to tune the heat flux at the mirror surface, and different thermocouples (TC_x) are utilized. The maximum bearable current in the variac is 8 A. Two mass flow meters were employed, with different ranges and uncertainties, as reported in Table I together with the pressure transducer and thermocouples.

To perform the thermal tests, the experimental setup was modified. Ten thermocouples were positioned on the surface of the mirror using glue and copper tape, as shown in Fig. 7(a).

This article has been accepted for inclusion in a future issue of this journal. Content is final as presented, with the exception of pagination.

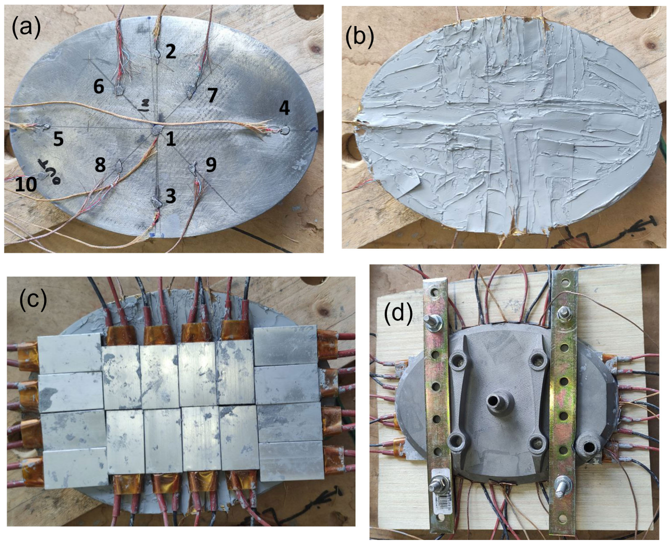

Fig. 7. Thermal test setup. (a) Thermocouples. (b) Silicon thermal paste on the mirror surface. (c) PTC resistors. (d) Resistors covered with rock wool and blocked with a wood plate.

To create a constant heat flux source, 16 positive temperature coefficient (PTC) resistors were placed on the surface [Fig. 7(c)], interposed with a silicon thermal paste [Fig. 7(b)]. The thermocouples were placed so as to avoid being directly below a heating element, but between two adjacent resistors, such that the reading of the mirror wall temperature should not be affected by the surface temperature of the heaters. To ensure that the resistors and the thermocouples were fixed to the surface, a pressed wood plate was secured to the mirror using screws, pressing the resistors and thermocouples, as shown in Fig. 7(d). The PTC resistors were connected as two parallel series of eight resistors to the variac.

Finally, the mirror was then thermally insulated, on both sides, by rock wool 10-cm thick, with a thermal conductivity of approximately 0.03 W/(m K), and connected to the same circuit of the hydraulic tests.

Referring to Fig. 7(a), *TC1* is located in the mirror center, and *TC2-3* and *4-5* are positioned along the minor and major axis, respectively. *TC6-9* are positioned diagonally with respect to the axes and *TC10* is placed in correspondence of the outlet. It should be noted that *TC2-3* are placed outside the resistors, thus they are expected to measure quite low temperatures.

Different nominal flow rates, spanning from 1.5 to 5.2 L/min, were tested at two power levels, with nominal voltages of 84 and 94 V, respectively. The flow rates and power levels are reported in Table II. The imposed power $\dot{Q}_c$ is computed from an energy balance as in (3), where $\dot{m}$ is the mass flow rate, c_p the specific heat capacity, and ΔT_{io} the temperature increase from inlet to outlet. The uncertainties of $\dot{Q}_c$ range between 10% and 30%. The power computed from the energy balance was compared for consistency to the electrical power $\dot{Q}_e$ as in (4) where ΔV is the imposed potential difference to the resistors' ends and I the current through the two series of resistors, measured using a current clamp. The average water inlet temperature is 20 °C. The calorimetric and

TABLE II
TESTED CONDITIONS IN THE THERMAL EXPERIMENTS

84 V

$\dot{V}$ (l/min)	$\dot{Q}_c$ (W)	$\dot{Q}_e$ (W)
1.48	**430 ± 50**	**450 ± 30**
1.77	**460 ± 50**	**460 ± 30**
2.57	420 ± 70	430 ± 30
2.59	440 ± 80	450 ± 30
3.34	460 ± 100	440 ± 30
3.46	520 ± 150	480 ± 30
4.17	490 ± 140	450 ± 30
4.30	470 ± 130	440 ± 30
4.88	**460 ± 140**	**440 ± 30**
5.18	**510 ± 160**	**440 ± 30**

94 V

$\dot{V}$ (l/min)	$\dot{Q}$ (W)	$\dot{Q}_e$ (W)
1.77	**580 ± 70**	**670 ± 40**
2.19	**610 ± 60**	**660 ± 40**
2.69	660 ± 80	680 ± 40
2.55	650 ± 80	660 ± 40
2.63	630 ± 80	640 ± 40
3.41	700 ± 100	690 ± 40
3.40	660 ± 100	670 ± 40
3.31	670 ± 110	640 ± 40
4.23	700 ± 120	690 ± 40
4.19	680 ± 120	680 ± 40
4.20	700 ± 140	660 ± 40
5.06	**670 ± 180**	**690 ± 40**
5.02	**640 ± 170**	**650 ± 40**
4.81	**670 ± 140**	**630 ± 40**

electrical power resulted in the same within their uncertainty bars, see Table II. It must be noted that the resistance characterization of the PTC resistors in a thermostatic bath was not possible because of their nonimpermeability

$$\dot{Q}_c = \dot{m} c_p \Delta T_{io} \quad (3)$$

$$\dot{Q}_e = 2 \Delta V I. \quad (4)$$

In both hydraulic and thermal tests, each test was recorded for 180 s at a frequency of 1 Hz. Between each thermal test, the variac was switched off, and the thermocouples were allowed to return to room temperature before continuing. After switching on the variac, several minutes were required for the system to reach a steady state, while monitoring the thermocouples, before starting data acquisition.

B. Simulation Setup

In the simulations, the same numerical setup exposed in Section II-B has been employed. For the modeling of the hydraulic experiments, isothermal conditions were used, and no external flux was imposed. The pressure drop between the inlet and outlet of the mirror, as in Fig. 1(a), has been extracted and compared to the experimental values. For the thermal tests, to mimic the heating from the PTC resistors, a constant heat flux of the same shape as the resistors was imposed. To reproduce the same conditions of the experiments, the imposed heat flux was computed from the calorimetry values of Table II as $\dot{Q}_c / A_{HL}$, where A_{HL} is the heated area. Because the experimental temperature increases were limited, both fluid and solid properties have been considered constant in the model.

This article has been accepted for inclusion in a future issue of this journal. Content is final as presented, with the exception of pagination.

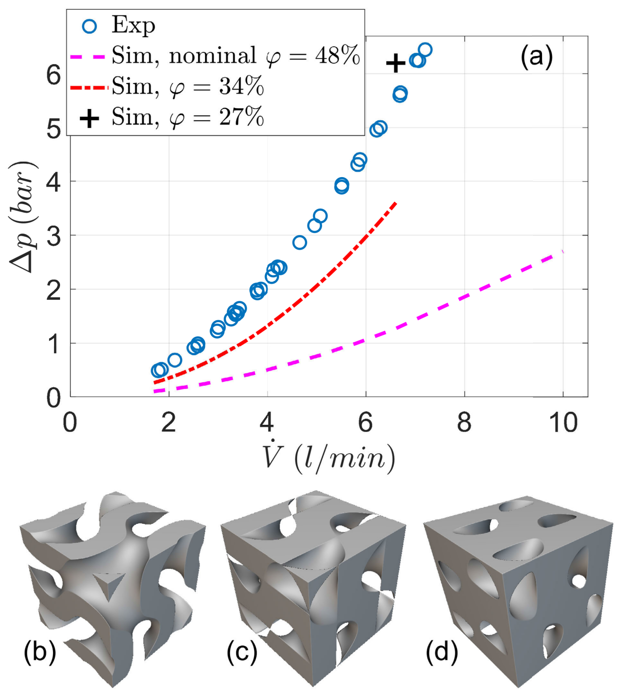

Fig. 8. Comparison of experimental and numerical results. (a) Pressure losses and gyroid unit cells at different porosities, (b) nominal 48%, (c) 34%, and (d) 27%.

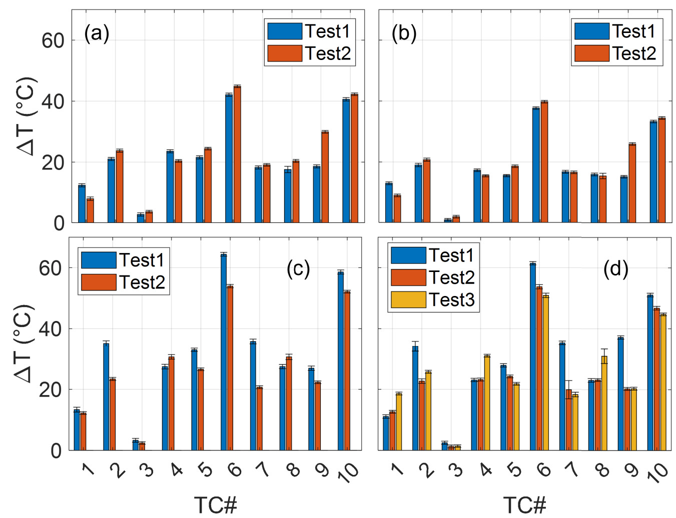

Fig. 9. Measured temperature increases for the smallest and largest flow rates at the two nominal powers. (a) 1.48–1.77 L/min and 84 V, (b) 4.88–5.18 L/min and 84 V, (c) 1.77–2.18 L/min and 94 V, and (d) 5.06–5.02-4.81 L/min and 94 V.

C. Hydraulic Tests

The pressure losses in the mirror are computed as the difference between the measured pressures at the inlet and outlet of the test section. Note that the influence of the pipes and connectors between the mirror and the pressure transducers was also investigated by removing the mirror from the circuit, and negligible effects were revealed. The comparison between the numerical and experimental results is shown in Fig. 8. As both the pressure drop and flow rate uncertainty are lower than 5% and 1% respectively, they are omitted from the chart for graphical clarity. While the experimental pressure drops measured during tests employing the two flow meters agree, there is a large discrepancy between the tests [blue curve in Fig. 8(a)] and the simulations for the nominal geometry [magenta curve in Fig. 8(a)].

Although an underestimation of the simulations compared to the measured hydraulic characteristics is expected—primarily due to the inherent roughness introduced by the printing method, which is quite difficult to capture accurately in the numerical model—the observed discrepancy is too significant to be explained by surface roughness alone.

Regarding the printing accuracy provided by the manufacturer, simulations were also carried out considering an effectively smaller lattice porosity, by increasing the wall thickness of the TPMS cell in the numerical simulations, as shown in Fig. 8(b)–(d). Increasing the wall thickness by 0.2 mm, thus decreasing φ from 48% to 34%, results in the computed red dotted curve in Fig. 8(a), considerably closer to the experimental curve. By further reducing the porosity down to 27%, the curve is slightly exceeded, as noted by the black cross (just one point was simulated for computational cost issues). A second look at Fig. 8 allows noting that, with the hypothesis of porosity decrease, the topology of the Gyroid structure appears deformed and eventually fluid passages are totally choked at some locations. Thus, the discrepancy between the experimental and simulation results could be attributed to printing tolerances/defects or local obstructions. A tomography could possibly confirm the speculation about the reduced effective porosity, and help in understanding to what extent the internal polishing by abrasive jet [22] could help in reducing the hydraulic impedance of the mirror, increasing the lattice porosity [23], [24].

D. Thermal Tests

For the thermal experiments, the temperature increase ΔT has been computed as follows with respect to the inlet temperature:

$$\Delta T = T_{TC} - T_{in}. \tag{5}$$

The evaluation of the standard uncertainty of the measurements has been performed by following the guidelines provided by the Joint Committee for Guides in Metrology [25].

The uncertainty of the measurand estimate $u(T_{TC})$ has been calculated by combining the statistical uncertainties from the random oscillations $[u_A(T_{TC})]$ in the experiments and the accuracy of the instrumentation $[u_B(T_{TC})]$ in (6). In particular, u_B is evaluated considering a uniform probability distribution. The uncertainty of the temperature increase has been computed with the propagation of uncertainty as in (7)

$$u(T) = \sqrt{u_A^2 + u_B^2} \tag{6}$$

$$u(\Delta T) = \sqrt{u^2(T_{TC}) + u^2(T_{in})}. \tag{7}$$

The ΔT measured by the different thermocouples is plotted in Fig. 9 for the smallest and largest flow rates and the two nominal potential differences. The setpoints are highlighted in bold in Table II. Looking at the measured data, if *TC3* has

This article has been accepted for inclusion in a future issue of this journal. Content is final as presented, with the exception of pagination.

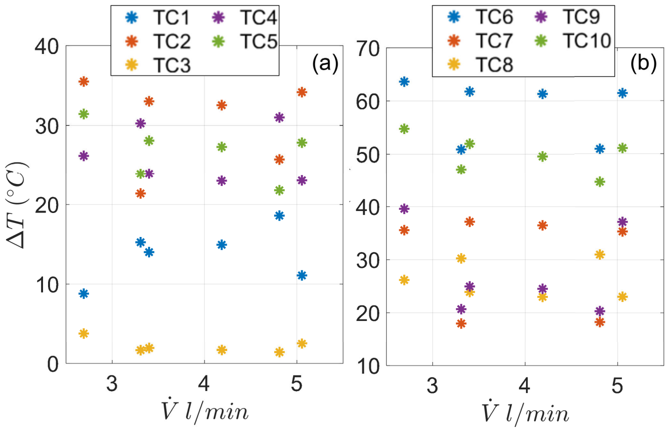

Fig. 10. Measured temperature increase as a function of the flow rate, at approximately the same power of 670 W. (a) *TC1-5* and (b) *TC6-10*.

the smallest temperature increase, *TC2* measures a quite large value, which could possibly be explained by a local occlusion within the mirror cooling structure. Consistent with its position at the inlet, *TC1* has a small temperature rise compared to the other thermocouples. *TC4* and *TC5* are at a specular position along the major axis, with *TC5* nearer to the outlet, thus expected lower measured temperature. This expectation is only partially verified as *TC5* is not always lower than *TC4*. In general, TC4 and TC5 have close values, but even considering the uncertainty, there is no compatibility in the measurements. Concerning *TC7-8-9*, they appear similar but completely off-range with respect to *TC6*, which is nonetheless in a specular position, and detects the highest temperature of the entire mirror.

The only thermocouple surely placed under a heating element was the *TC10*, thus its reading could be the most affected by the temperature of the resistors.

In Fig. 10, six flow rates have been selected, cooling approximately the same amount of power around 670 W. In this way, the effect of flow rate on temperature measurements is directly investigated.

While it would be expected that, as the flow rate increases, heat exchange would increase, thereby decreasing the temperatures read by the thermocouples, it is clear that this decreasing trend is not present. This brings into question the actual suitability of the experimental setup, which is probably overly biased by the heating elements, which, despite the use of thermal paste and compression against the mirror surface, were hotter than the metal surface.

In order to compare the thermal efficiency of the mirror in the different tests from an average perspective, a modified heat transfer coefficient H^* has been calculated as follows:

$$H^* = \frac{\dot{Q}}{A_{HL}(T_{HL} - T_{in})}. \quad (8)$$

T_{HL} is the mean temperature on the mirror surface, where the heat load is applied. T_{HL} has been computed as a weighted average of the *TC* readings, by considering they affect different portions of the mirror surface, as in Fig. 11. H^* should be regarded as a sort of global heat transfer coefficient, measuring the ability of the TPMS-based cooling system to remove power

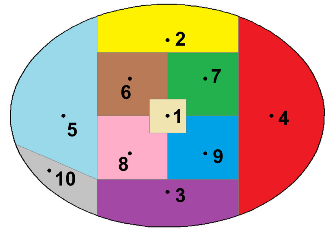

Fig. 11. Mirror surface divided into sectors for T_{HL} computation.

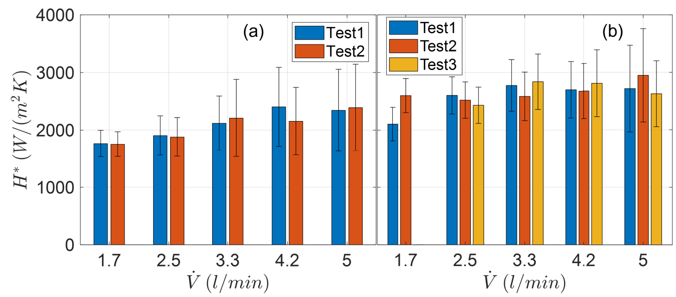

Fig. 12. Comparison of thermal performance of the experimental and numerical results through the heat transfer coefficient. (a) ΔV = 84 V and (b) ΔV = 94 V. The x label refers to the nominal values of flow rates.

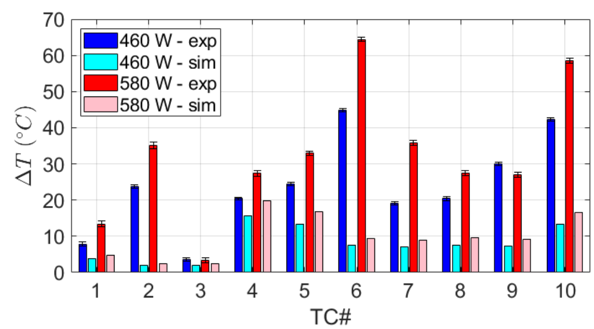

Fig. 13. Comparison between simulations and experiments: measured temperature increase at 1.77 L/min and 460–580 W.

from the mirror surface in the different tests and allowing the comparison of results at different flow rates and heat loads. However, it remains an approximation of an actual global heat transfer coefficient, as the temperature of the mirror's heated surface was not uniform. In theory, H^* should increase with the flow rate, as the larger velocity raises the convective heat removal, and remain constant with the heat flux, considering that the mirror material has practically constant properties within these temperature windows.

The results are shown in the bar plot of Fig. 12. At approximately the same flow rate and power, the H^* values are within the uncertainty ranges, which was not the case for Fig. 9. Furthermore, there is a slight increase in H^* with flow rate, but again, this is unclear and within the range of uncertainty.

Note also that, at the nominal potential difference of 94 V, the values of H^* are larger than those computed at 84 V, whereas they were expected to be the same. This is again an indication that the influence of the resistors in the thermocouple readings is not negligible.

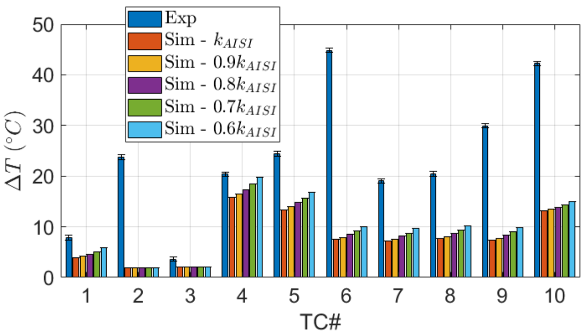

Fig. 14. Effect of the thermal conductivity on the numerical results.

In Fig. 13, the experimental measurements are compared to the simulation results at the lowest flow rate and two power levels. By increasing the power level, the thermocouples' readings increase, both in the numerical and experimental results. However, the simulated temperatures are dramatically lower than in the experiments and cannot be explained by the experimental uncertainty of the *TC*. The two simulations at the same flow rate and different power levels can also be considered as a sensitivity analysis on the effect of power on *TC*. In fact, the relative increase between 460 and 580 W of 26% is similar to the uncertainties in the computed $\dot{Q}_c$, and yet it does not lead to sufficient increases in the simulation temperatures to explain the numerical–experimental difference.

An effect that has been parametrically investigated to help explain the difference between the experimental and computed temperature increase is related to the thermal conductivity of the stainless steel. In the simulations, the bulk material conductivity k_{AISI} has been used (taken from the ITER database [26]), whereas the conductivity of the prototype resulting from the LPBF manufacturing process could be reduced compared to the bulk value [27], [28]. The results of the parametric analysis are shown in Fig. 14.

Decreasing the conductivity of the stainless steel to 0.6 of its bulk value leads to temperature increases of 20%–50% depending on the thermocouple, which is not sufficient to explain the numerical–experimental difference in the thermocouple readings. The nonsignificant increase in *TC2-3* is due to their positions outside the heating elements' location. These preliminary thermal results highlighted some experimental limitations and did not allow a full validation of the model, even though different hypotheses have been proposed to interpret the measurements.

V. Conclusion and Perspective

In this article, a TPMS-based cooling system has been successfully designed for the prototype of the M2 mirror of DTT ECH system, to be tested at Falcon facility. The component has been simulated to verify the compliance with the requirements of the facility, and then realized via SLM in AISI 316L. Both the printing and depowdering processes proved successful. A dedicated hydraulic setup was also developed, and the prototype was tested, enabling a first experimental check of the numerical hydraulic and thermal models. The measured pressure losses within the prototype mirror were much larger than the simulated ones, as previously found in literature for metal-printed samples, possibly due to roughness, printing accuracy, or local occlusions. The high experimental pressure drop could be only reproduced numerically if an effective porosity of 27% was assumed. Tomographic analyses may help in the future to verify the numerical hypotheses of effective porosity reduction.

The thermal behavior of the mirror, including also the experimental assessment of the thermal conductivity of the 3-D-printed stainless steel, requires further investigation.

Further experiments need to be carried out with a different setup, for example, with a solar simulator such as the IMDEA facility in Madrid [29] and thermal sensors that are not influenced by the heating elements, such as fiber optics [30].

The use of the abrasive jet polishing method is planned for the mirror prototype in the future to evaluate its effectiveness in completing the finishing process of the additively manufactured part.

Acknowledgment

The authors acknowledge the use of computational resources provided by HPC@Polito, which is a project of Academic Computing within the Department of Control and Computer Engineering at the Politecnico di Torino, Turin, Italy (http://www.hpc.polito.it).

References

[1] V. Erckmann and U. Gasparino, "Electron cyclotron resonance heating and current drive in toroidal fusion plasmas," *Plasma Phys. Control Fusion*, vol. 36, no. 12, pp. 1869–1962, 1994.
[2] M. K. A. Thumm, G. G. Denisov, K. Sakamoto, and M. Q. Tran, "High-power gyrotrons for electron cyclotron heating and current drive," *Nucl. Fusion*, vol. 59, no. 7, Jul. 2019, Art. no. 073001.
[3] F. Fanale et al., "Status of DTT ECH transmission lines and antennae," *IEEE Trans. Plasma Sci.*, vol. 52, no. 9, pp. 3778–3784, Sep. 2024.
[4] F. Romanelli et al., "Divertor tokamak test facility project: Status of design and implementation," *Nucl. Fusion*, vol. 64, no. 11, 2024, Art. no. 112015.
[5] G. Granucci et al., "The DTT device: System for heating," *Fusion Eng. Design*, vol. 122, pp. 349–355, Nov. 2017.
[6] K. Sakamoto et al., "Development of high power gyrotron for ITER application," in *Proc. 35th Int. Conf. Infr., Millim., THz Waves*, Sep. 2010, pp. 1–2.
[7] Z. C. Ioannidis et al., "First CW experiments with the EU ITER 1 MW, 170 GHz industrial prototype gyrotron," in *Proc. 18th Int. Vac. Electron. Conf. (IVEC)*, Apr. 2017, pp. 1–2.
[8] Z. C. Ioannidis et al., "Recent experiments with the European 1MW, 170 GHz industrial CW and short-pulse gyrotrons for ITER," *Fusion Eng. Des.*, vol. 146, pp. 349–352, Sep. 2019.
[9] F. Braunmueller et al., "Results on the 1 MW CW 170 GHz gyrotron TH1509UA for ITER and DTT at the FALCON test stand," in *Proc. EPJ Web Conf.*, vol. 313, 2024, p. 04005.
[10] F. Fanale et al., "Progress on the conceptual design of the antennas for the DTT ECRH system," *Fusion Eng. Design*, vol. 192, Jul. 2023, Art. no. 113797.
[11] D. Busi et al., "Study of magnetic effects on DTT ECRH front-steering mirror," *Fusion Eng. Des.*, vol. 191, Jun. 2023, Art. no. 113550.
[12] A. Allio et al., "Assessment of the performance of different cooling configurations for the launcher mirrors of the ECRH system of the DTT facility," *IEEE Trans. Plasma Sci.*, vol. 50, no. 11, pp. 4054–4059, Nov. 2022.
[13] L. Savoldi, A. Cammi, W. Ferretto, A. Quamori Tanzi, and L. Marocco, "Use of triply periodic minimal surface lattices for heat transfer applications: A systematic literature investigation," *Energies*, vol. 19, no. 3, p. 833, Feb. 2026.

This article has been accepted for inclusion in a future issue of this journal. Content is final as presented, with the exception of pagination.

[14] E. Gajetti et al., "A new efficient mirror cooling for the transmission line of fusion reactor ECH systems based on triply periodic minimal surfaces," *IEEE Trans. Plasma Sci.*, vol. 52, no. 9, pp. 3765–3771, Sep. 2024.

[15] M. G. Gado, O. Al-Ketan, M. Aziz, R. A. Al-Rub, and S. Ookawara, "Triply periodic minimal surface structures: Design, fabrication, 3D printing techniques, state-of-the-art studies, and prospective thermal applications for efficient energy utilization," *Energy Technol.*, vol. 12, no. 5, May 2024, Art. no. 2301287.

[16] A. Quamori Tanzi, A. Cammi, L. Marocco, and L. Savoldi, "Design of a 10 MW/m2-heat-flux removal system for a W7-X divertor tile using triply periodic minimal surfaces," *Case Stud. Thermal Eng.*, vol. 63, Nov. 2024, Art. no. 105405.

[17] S. Garavaglia et al., "First RF operations of the gyrotron for the DTT ECRH system," *Fusion Eng. Design*, vol. 222, Jan. 2026, Art. no. 115488.

[18] *Siemens Digital Industries Software, 'Simcenter STAR-CCM+, Version 2310.001'*, Siemens Digit. Industries Softw., Plano, TX, USA, 2023.

[19] T. Dudziak et al., "Effect of 316L stainless steel fabrication on oxidation resistance, surface morphology, and hot tensile behavior," *J. Mater. Eng. Perform.*, vol. 32, no. 22, pp. 10443–10454, Nov. 2023.

[20] *National Institute of Standards and Technology, U.S: Department of Commerce*. Accessed: Oct. 16, 2025. [Online]. Available: https://webbook.nist.gov/chemistry/fluid/

[21] F. Ternero, L. G. Rosa, P. Urban, J. M. Montes, and F. G. Cuevas, "Influence of the total porosity on the properties of sintered materials—A review," *Metals*, vol. 11, no. 5, p. 730, Apr. 2021.

[22] F. Davoodi, M. Taghian, G. Carbone, A. Saboori, and L. Iuliano, "An overview of the latest progress in internal surface finishing of the additively manufactured metallic components," *Materials*, vol. 16, no. 10, p. 3867, May 2023.

[23] K. Yan, H. Deng, Y. Xiao, J. Wang, and Y. Luo, "Thermo-hydraulic performance evaluation through experiment and simulation of additive manufactured gyroid-structured heat exchanger," *Appl. Thermal Eng.*, vol. 241, Mar. 2024, Art. no. 122402.

[24] K. Yan, H. Deng, Y. Xiao, J. Wang, Y. Luo, and J. Yan, "Influence of polishing process on surface morphology and thermo-hydraulic performance of additively manufactured gyroid-structured heat exchanger," *Appl. Thermal Eng.*, vol. 253, Sep. 2024, Art. no. 123828.

[25] *JCGM 100:2008. Evaluation of Measurement Data-guide to the Expression of Uncertainty in Measurement*, BIPM, IEC, IFCC, ILAC, ISO, IUPAC, IUPAP and OIML, Sèvres, France, 2008.

[26] J. W. Davis, "Iter material properties handbook," Oak Ridge Nat. Lab. (ORNL), Oak Ridge, TN, USA, Tech. Rep. DOE/ER–0313/16, 1994. [Online]. Available: https://www.osti.gov/biblio/47735

[27] F. Eichler, N. Balc, S. Bremen, and P. Nink, "Investigation of laser powder bed fusion parameters with respect to their influence on the thermal conductivity of 316L samples," *J. Manuf. Mater. Process.*, vol. 8, no. 4, p. 166, Aug. 2024. [Online]. Available: https://www.mdpi.com/2504-4494/8/4/166

[28] J. C. Simmons et al., "Influence of processing and microstructure on the local and bulk thermal conductivity of selective laser melted 316L stainless steel," *Additive Manuf.*, vol. 32, Dec. 2019, Art. no. 100996. [Online]. Available: https://www.sciencedirect.com/science/article/pii/S2214860419314381

[29] J. Li, J. González-Aguilar, and M. Romero, "Line-concentrating flux analysis of 42kWe high-flux solar simulator," *Energy Proc.*, vol. 69, pp. 132–137, May 2015. [Online]. Available: https://www.sciencedirect.com/science/article/pii/S1876610215003227

[30] S. Zhou et al., "Sub-millisecond response fiber-optic temperature sensor based on microfabricated silicon Fabry–Pérot interferometer," *Opt. Fiber Technol.*, vol. 95, Dec. 2025, Art. no. 104401. [Online]. Available: https://www.sciencedirect.com/science/article/pii/S1068520025002767

Eleonora Gajetti received the M.Sc. degree (cum laude) in energy and nuclear engineering (specialization: sustainable nuclear energy) from Politecnico di Torino, Turin, Italy, in 2022, where she is currently pursuing the Ph.D. degree in energetics.

Her master's internship at Thales AVS, Vélizy-Villacoublay, France, related to Gyrotron cooling systems. Her research interests include the development of advanced cooling systems for components subjected to high heat fluxes in the nuclear fusion field.

Alessandro Bruschi, photograph and biography not available at the time of publication.

Francesco Fanale, photograph and biography not available at the time of publication.

William Ferretto, photograph and biography not available at the time of publication.

Gustavo Granucci, photograph and biography not available at the time of publication.

Andrea Lucchini, photograph and biography not available at the time of publication.

Luca Marocco, photograph and biography not available at the time of publication.

Afra Romano, photograph and biography not available at the time of publication.

Laura Savoldi (Senior Member, IEEE) received the M.Sc. degree (cum laude) in nuclear engineering and the Ph.D. degree in energetics from Politecnico di Torino, Turin, Italy, in 1997 and 2001, respectively.

She currently serves as a Full Professor in nuclear plants at Politecnico di Torino. She has authored or co-authored over 200 articles published in international journals and proceedings of international conferences. Her research interests include the development, validation, and application of computational tools for the analysis of thermal-hydraulic transients in advanced heat transfer problems, including superconducting magnets and high heat flux components. In this frame, she developed the 4C code for the analysis of thermal–hydraulic transients in superconducting cables, coils, and related cryogenic circuits.

Prof. Savoldi serves as a referee for several international journals and conferences in her field of research, among which IEEE Transactions on Applied Superconductivity and IEEE Transactions on Plasma Science.

Open Access funding provided by 'Politecnico di Torino' within the CRUI CARE Agreement